A Contactless Health Monitoring System for Vital Signs Monitoring, Human Activity Recognition and Tracking

Anna Li, Eliane Bodanese, Stefan Poslad, Penghui Chen, Jun Wang, Yonglei Fan, Tianwei Hou

***Abstract*—Integrated sensing and communication technologies provide essential sensing capabilities that address pressing challenges in remote health monitoring systems. However, most of today's systems remain obtrusive, requiring users to wear devices, interfering with people's daily activities, and often raising privacy concerns. Herein, we present HealthDAR, a low-cost, contactless, and easy-to-deploy health monitoring system. Specifically, HealthDAR encompasses three interventions: i) Symptom Early Detection (monitoring of vital signs and cough detection), ii) Tracking & Social Distancing, and iii) Preventive Measures (monitoring of daily activities such as face-touching and handwashing). HealthDAR has three key components: (1) A low-cost, low-energy, and compact integrated radar system, (2) A simultaneous signal processing combined deep learning (SSPDL) network for cough detection, and (3) A deep learning method for the classification of daily activities. Through performance tests involving multiple subjects across uncontrolled environments, we demonstrate HealthDAR's practical utility for health monitoring.**

***Index Terms*—Deep learning, Integrated sensing and communication, Radar, Remote health monitoring**

I. INTRODUCTION

INTEGRATED sensing and communication (ISAC) technologies offer a compelling avenue for exploiting wireless and hardware resources for dual-purpose applications [1]. Future wireless networks are anticipated to be extremely dense, with billions of connected devices continuously exchanging signals [2]. This density could be harnessed to achieve pervasive sensing capabilities at almost zero cost [3]. The importance of such technology is clearly highlighted when considering the challenges faced by global healthcare systems.

This work was supported in part by the National Natural Science Foundation for Young Scientists of China under Grant 62201028, in part by the Fundamental Research Funds for the Central Universities under Grant 2023JBZY012, in part by Young Elite Scientists Sponsorship Program by CAST under Grant 2022QNRC001, and in part by supported by the Marie Skłodowska-Curie Fellowship under Grant 101106428. (Corresponding author: Yonglei Fan.)

Anna Li is with the School of Computing and Communications, Lancaster University, Lancaster LA1 4WA, U.K. (e-mail: a.li16@lancaster.ac.uk).

Eliane Bodanese, Stefan Poslad and Yonglei Fan are with School of Electronic Engineering and Computer Science, Queen Mary University of London, London E1 4NS, U.K. (e-mail: eliane.bodanese@qmul.ac.uk, stefan.poslad@qmul.ac.uk, yonglei.fan@qmul.ac.uk).

Penghui Chen and Jun Wang are Electronic Information Engineering, Beihang University, Beijing 100190, China. (e-mail: chenpenghui@buaa.edu.cn, wangj203@buaa.edu.cn).

Tianwei Hou is with the School of Electronic and Information Engineering, Beijing Jiaotong University, Beijing 100044, China, and also with the Institute for Digital Communications, Friedrich-Alexander Universität Erlangen-Nürnberg (FAU), 91054 Erlangen, Germany. (email: twhou@bjtu.edu.cn).

Recent years have witnessed the emergence of wearable technologies for non-invasive health monitoring [4]–[6]. However, these wearable devices can be uncomfortable, expensive, and limited in usage, necessitating direct attachment to the person's skin or body. For instance, the elderly often feel encumbered or embarrassed by wearable devices, and individuals with dementia might forget to wear them. Infants are at risk of skin irritation from wearable sensors, while patients with severe burn wounds find them difficult to tolerate. Furthermore, these devices require the user to remember daily recharging. A health monitoring method must meet criteria for large-scale, everyday use, prompting the healthcare industry to shift its focus gradually towards contactless remote health monitoring solutions. While camera-based solutions [7] can directly monitor daily human activities, they struggle to capture vital signs. They are also limited by variability in brightness, contrast, and exposure, and they potentially raise privacy concerns [8].

Much attention has been recently given to healthcare using the radio frequency (RF) sensing modality [9], [10], [10]–[15]. Radar sensors are contactless devices capable of operating under any lighting conditions, and can penetrate opaque objects such as tables or walls [16]. An additional feature that renders radar particularly attractive for health monitoring is its adherence to privacy norms for monitored individuals, making it suitable for environments like hospitals, restrooms, bedrooms, and other locations where the presence of video cameras would be discomforting. Driven by advances in machine learning and hardware-software integration, radars are uniquely positioned to provide insights into long-term monitoring of evolving body states, offering a sense of security and safety for individuals [17].

A. Objectives and motivations

The development of millimeter-wave (mmWave) communication technologies opens up new avenues for catering to sensing applications that have more rigorous demands [18]. Utilizing the substantial bandwidth inherent in mmWave communication systems can significantly enhance the sensing resolution, particularly in range measurements [19]. In this paper, we concentrate on the sensing aspect of ISAC, particularly emphasizing remote health monitoring. We have devised a comprehensive sensing platform that employs radar technology for high-precision sensing, delivering crucial, reliable data for remote health monitoring. This platform acts as a testbed

This article has been accepted for publication in IEEE Internet of Things Journal. This is the author's version which has not been fully edited and content may change prior to final publication. Citation information: DOI 10.1109/JIOT.2023.3336232

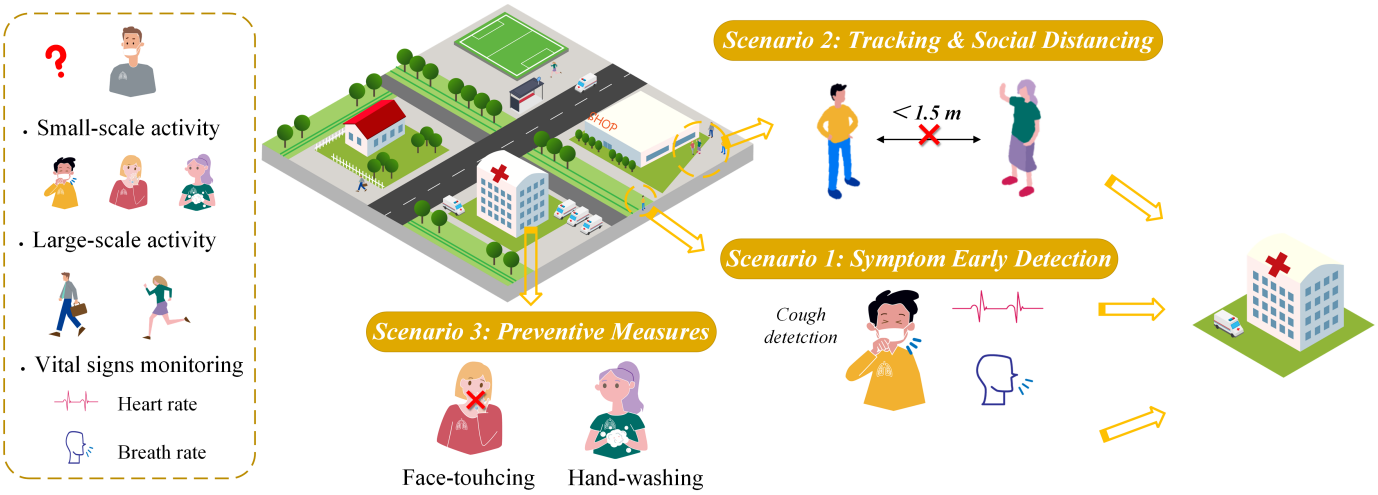

Fig. 1: Application Scenarios.

to evaluate sensing efficacy. Specifically, our objective is to introduce HealthDAR, a remote health monitoring system that requires only a 'coin-sized' radar (22 mm × 44 mm), making it suitable for deployment in homes, offices, malls, and other similar settings. HealthDAR operates unobtrusively, without interfering with individuals' daily activities, without invading their privacy. This makes it well-suited for environments such as hospitals, restrooms, and bedrooms, where the use of cameras would be considered intrusive. The World Health Organization (WHO) has stressed the necessity for early detection of infectious diseases and outlined effective preventive measures, including frequent hand washing, social distancing, and avoiding face touching [20]. To better follow these instructions, we consider three scenarios supported by HealthDAR, as shown in Fig. 1: i) Symptom Early Detection, ii) Tracking & Social Distancing, and iii) Preventive Measures. We have several motivations for each considered scenario:

- Symptom Early Detection: Vital signs (heart rate and breath rate) are essential for illustrating the physical condition of individuals, where abnormal breathing patterns and irregular heart beat could indicate the potential of infectious disease. Cough detection holds critical importance, as coughing significantly contributes to the transmission of viruses through airborne droplets [21]. Therefore, reliable early diagnosis based on cough analysis, complemented by vital signs, would offer a swift and convenient method for controlling the spread of infectious diseases in a pandemic situation [22]. Most preceding studies in cough detection [23]–[25] utilized short-term magnitude spectrograms, transformed from cough sound data by deep learning models. However, these are susceptible to background noise, which could be misinterpreted as cough sounds [26]. Moreover, audio-based solutions raise privacy concerns.
- Tracking & Social Distancing: Sensing location information can help identify areas that are at risk of virus exposure and remind people to keep social distancing [29]–[31]. Since existing studies usually target one person, it is challenging to track the location of a cough in public places with many people. In addition, many previous studies have focused on wearable devices, which required users to wear a 'tag', use an active mobile device such as a smartphone [32], or install equipment such as microphones [33]. These solutions may cause inconvenience for some users.
- Preventive Measures: There is a significant need to develop a health monitoring system that actively reminds individuals to adhere to proper hygiene practices, such as frequent hand washing and avoiding face touching. Such practices are vital in maintaining health, and monitoring them involves detecting small-scale activities, characterized by micro-Doppler signatures (MDS). These MDS are generated by micro-movements of weak scattering points, typical of actions like hand-washing and face-touching. In contrast, larger-scale activities such as running or walking produce a different kind of Doppler signature, resulting from the movement of strong main scattering points, primarily the trunk. Both types of activities - small and large scale - can be analyzed using spectrograms, which effectively represent the state of human activity. Recently, deep learning algorithms have begun to automatically extract the most prominent MDS features from spectrograms, forgoing artificial feature extraction [34]. Many works [35]–[37] based on radars have successfully used different deep learning models to recognize different small-scale activities, but performance analysis under multi-people application scenarios in different environments remains an uncharted territory. Specifically, achieving high recognition accuracy of the micro-activities for new individuals in uncontrolled environments is highly challenging because this goal has to be met in multi-scenario settings with numerous sources of clutter and interference.

B. Implementation and Evaluations

We conducted our experiments on three subjects in two uncontrolled environments, both indoors and outdoors. We

This article has been accepted for publication in IEEE Internet of Things Journal. This is the author's version which has not been fully edited and content may change prior to final publication. Citation information: DOI 10.1109/JIOT.2023.3336232

TABLE I: Comparison of technologies measuring human large-scale activity, small-scale activity and vital signs.

	Contactless	Privacy Issues	Environment Adaptability	Large-scale Activity Accuracy	Small-scale Activity Accuracy	Vital Signs Accuracy
Wearable sensors [4]–[6]	×	×	Medium	High	High	High
Acoustic sensors [27], [28]	Depends	✓	Low	Low	Low	High
Cameras [7]	✓	✓	Low	High	High	-
Wi-Fi [13], [14]	✓	×	High	Low	Low	Low
This paper	✓	×	High	High	High	High

collected over 6000 samples, ranging from large-scale activities, small-scale activities, to vital signs. We then evaluated HealthDAR on 22 new (unseen) subjects. The results indicate that HealthDAR generalizes well to new (unseen) subjects. Specifically:

- The correlation between the test and ground truth for the heart rate (0.99) and breath rate (0.98) suggests that HealthDAR's results are highly correlated with the ground truth.
- The proposed simultaneous signal processing and deep learning (SSPDL) network provides 100% cough detection accuracy, resulting in a 49.7% and 1.4% improvement over AlexNet and DenseNet-201 (baselines), respectively. For new (unseen) subjects, an Equal Error Rate (EER) of 1.8% was achieved.
- HealthDAR achieves 100% overall accuracy (OA) on both face-touching and hand-washing in both indoor and outdoor scenarios, whether performed by one person or multiple people. This demonstrates that our approach is robust against changes in the environment or the number of people. When tested on new (unseen) subjects, although HealthDAR's accuracy experienced an average drop of 3.85%, it still maintained stable performance.

C. Contributions

In this paper, we focus on pure sensing, exploring the potential of RF for remote health monitoring in terms of symptom early detection, tracking & social distancing, and preventive measures. Our system does not necessitate users to actively provide input or to wear any devices on their bodies, making it comfortable and easy for everyone to use. Specifically, we simultaneously monitor daily activities, vital signs, and localization in practice, filling a gap in RF-based health monitoring. We precisely determined the locations and vital signs of multiple volunteers and successfully recognized their social distance in a real-world setting. We further evaluated the performance of the proposed system in recognizing face-touching and hand-washing, where the proposed system achieves 100% accuracy whether performed by one person or multiple people in uncontrolled environments. When tested on 22 unseen subjects, the proposed system continued to exhibit stable performance. This confirms that our approach is robust against varied scenarios or multiple users. In comparison with existing state-of-the-art solutions (shown in TABLE I), the proposed system represents a fully functional and innovative prototype, ready to unlock new possibilities across a wide spectrum of sensing applications.

D. Organization

The rest of the paper is organized as follows. Section II introduces the system design. Section III presents the detailed experimental setup. Section IV reports the evaluation results. Section V concludes this paper.

II. SYSTEM DESIGN

A. General architecture of the system

Here, we present a remote health monitoring system based on a Frequency-Modulated Continuous-Wave (FMCW) radar. It operates by transmitting wireless signals and measuring their reflections off the user's body. Fig. 2 shows schematic illustrations of the entire procedure for establishing the proposed health monitoring system. The developed system is composed of three modules that operate in a pipelined manner: hardware module, data processing module, and recognition module. Briefly, in the data processing module, signal processing methods are utilized to collect the original heartbeat signal, respiratory signal, micro-Doppler signatures, and four-dimensional (4D) radar data cube containing time-domain, sampling-domain, space-domain, and frame-domain information. In the recognition module, deep neural network classifiers are utilized for human activity recognition. Residual networks (ResNets) are presented for small-scale activity recognition, including coughing, hand-washing, and face-touching. The SSPDL algorithm is presented to detect cough by considering cough and vital signs jointly.

B. Hardware design

Three fundamental principles are adhered to in the hardware design: low-cost, low-energy, and low-space.

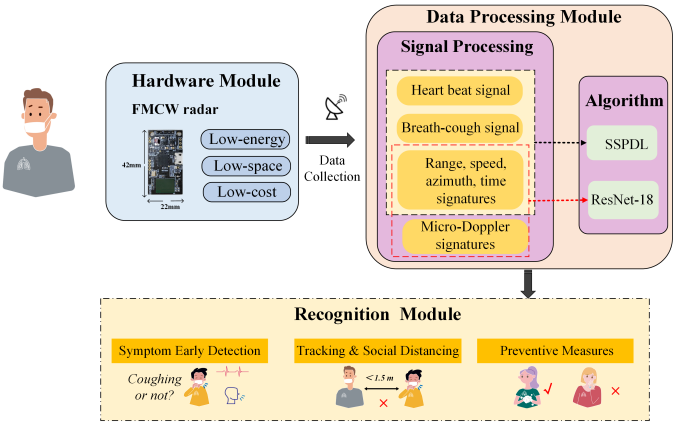

Fig. 2: System overview.

This article has been accepted for publication in IEEE Internet of Things Journal. This is the author's version which has not been fully edited and content may change prior to final publication. Citation information: DOI 10.1109/JIOT.2023.3336232

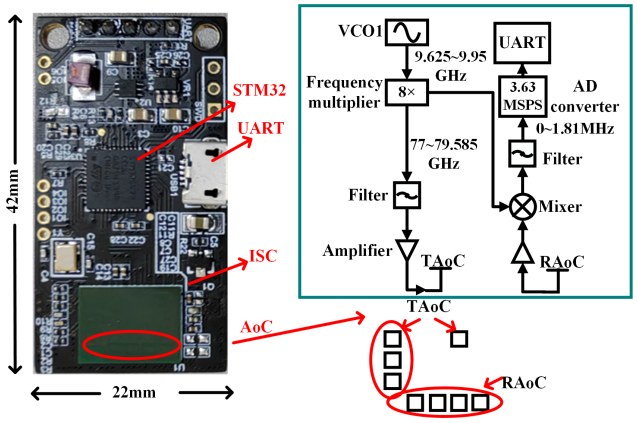

Fig. 3: The illustration of FMCW radar.

Low-cost: It requires a large number of radars for the proposed application scenarios, which indicates that the cost of each radar must be acceptable for deploying massive radar hardware. Normally, the current commercial FMCW radar in 77 GHz needs 200-400 USD, e.g., IWR1642Boost [38], and hence the funding requirement may be unacceptable for massive deployment. The cost of the whole equipment used in this paper could be lower than 20 USD for massive deployment.

Low-energy: In most of today's commercial FMCW radars, the power consumption is higher than expected. For example, if the radar requires a 12 voltage direct current (V-DC), then an adapter is necessary for each radar for transferring alternating current (AC) without any doubt. Hence, providing massive adapters is not realistic in practice and more energy consumption also enhances the cost of energy. To minimize the required energy of the presented FMCW radar, a simple USB interface from the laptop is utilized, facilitating both data transfer and power supply simultaneously.

Low-space: In practice, the space of the FMCW radar must be limited to the unspectacular level if we want to monitor human daily activities in public scenarios. The best way to meet the total space requirements of FMCW radar for avoiding extra attention is to integrate Voltage Controlled Oscillators (VCO), frequency multipliers, mixers, filters, amplifiers, Analog-to-digital (AD) converter, transmitting antennas, and receiving antennas into a single chip.

Based on the above-mentioned principles, the hardware of an FMCW radar used in this paper is illustrated in Fig. 3. As we can see from Fig. 3, only two major components, an STM32 series microprocessor and an integrated-sensing chip (ISC), are included in the hardware equipment. The STM32 series is a low-price microprocessor, where the price is normally lower than 1 USD. The ISC is designed and produced by ourselves, which includes VCO, frequency multipliers, mixers, filters, amplifiers, AD converter, and antennas. Conventionally, the antennas of mmWave signal are located on the Printed Circuit Board (PCB) directly. However, to minimize the required space of antennas, the transmitting antennas and receiving antennas are integrated into the ISC, namely transmitting-antenna-on-chip (TAoC) and receiving-antenna-on-chip (RAoC). A comparison of our hardware with some benchmark schemes is provided in Fig. 4, which better illustrates the size of our FMCW radar for readers. As can be seen in Fig. 4, the designed FMCW radar is even smaller than a Kingston flash disc.

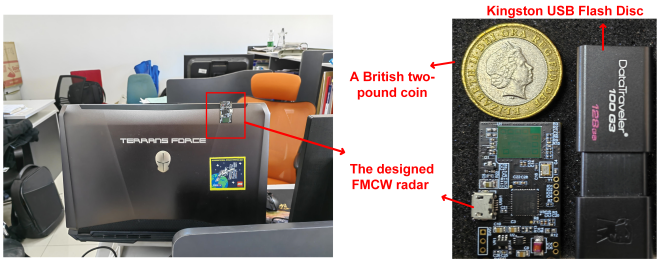

Fig. 4: The comparison between the IWR1642Boost, a flash disc, a British two-pound coin, and our FMCW radar.

The FMCW radar has two modes: work mode and data transmission mode. In the work mode, four TAoCs are activated one by one in a frame, each of which activates 1360 μs. The voltage and current of the work mode are 5 V and 310 mA, respectively. In the data transmission mode, both of TAoCs and RAoCs are inactivated, whereas only the universal asynchronous receiver transmitter (UART) is activated in the frame. In this case, the voltage and current of the data transmission mode are 5 V and 110 mA, respectively.

C. Signal waveform and processing

1) Signal waveform: We then turn our attention to the FMCW signal waveform as illustrated in Fig. 5. In our ISAC system, we simply involve the communication data into the sensing system by changing chirp slopes. Note that due to the constraint of the Microcontroller unit (MCU), we can only change the chirp slope in different fame, thus the maximum data rate can be simply derived as 25 bps. Since the memory of the ISC is not enough for massive waveforms, there is only one waveform available. In the work mode, VCO first generates a 9.625 GHz sine signal as the RF source. Then, the signal is multiplied by 8, and the output is a 77 GHz sine signal. The signal frequency of VCO linearly increases from 9.625 GHz to 9.95 GHz in T = 85 μs, and hence the output signal frequency increases from 77 GHz to 79.585 GHz, which is called a Chirp.

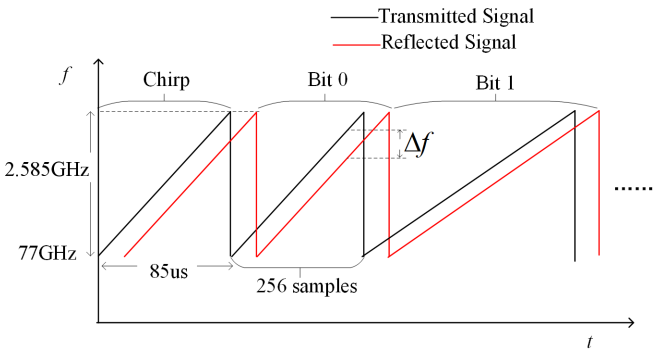

Fig. 5: The FMCW signal waveform.

This article has been accepted for publication in IEEE Internet of Things Journal. This is the author's version which has not been fully edited and content may change prior to final publication. Citation information: DOI 10.1109/JIOT.2023.3336232

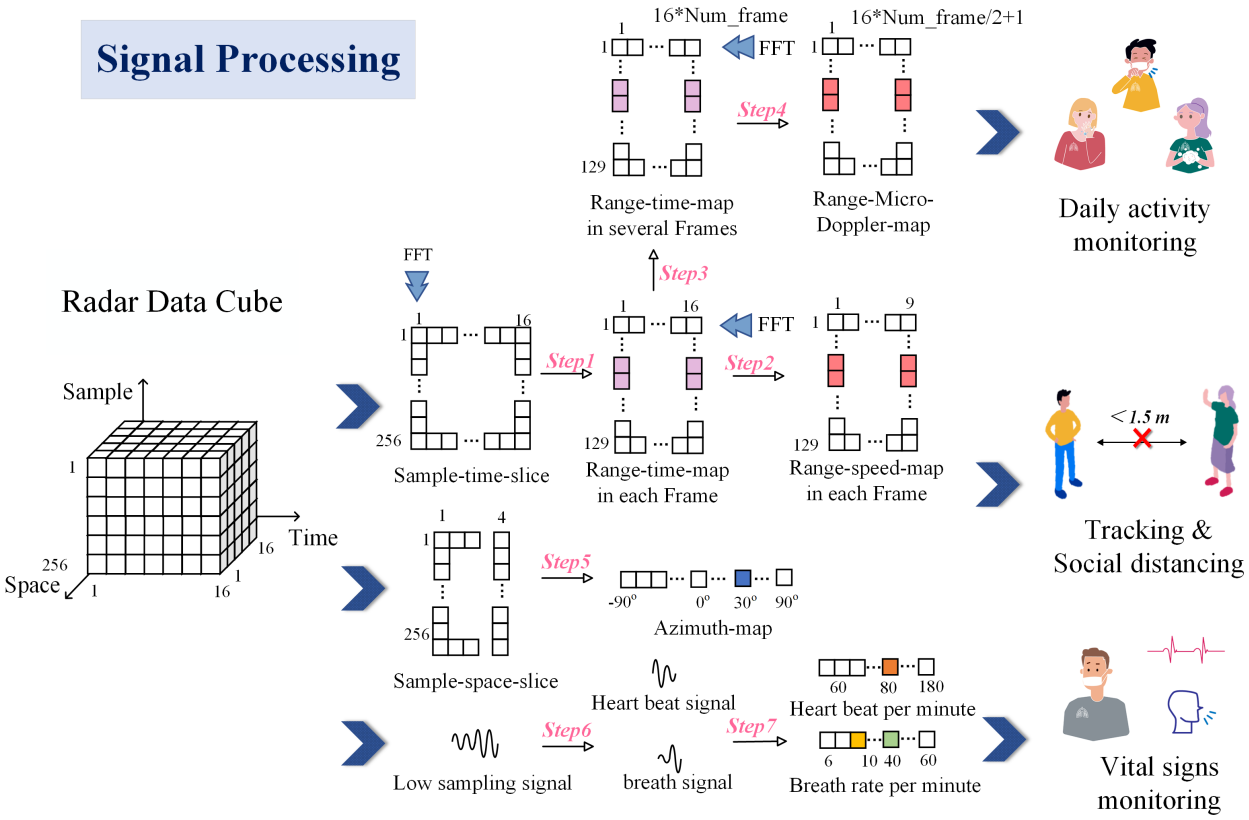

Fig. 6: The signal processing steps of collected data.

TABLE II: The parameter setting of our FMCW radar.

Parameters	Values
Effective bandwidth	$B = 2.585$ GHz
Carrier frequency	77 GHz
Number of Tx antennas	4
Number of Rx antennas	4
Antenna type	Antenna on chip
Chirp duration	$T = 85$ μs
Chirp slope	30.4118 MHz/μs
ADC sampling frequency	3.6363 MHz
Range resolution	0.070060 m
Maximum range	12.8 m
Frame time	40 ms

By utilizing the filter and amplifier, the generated FMCW signal is radiated by four TAoCs. Note that four TAoCs are activated one by one within different time resource blocks, whereas four RAoCs are simultaneously activated. By doing so, the FMCW radar is capable of evaluating both the azimuth and height of the detected target. The detailed parameters of the designed FMCW radar are concluded in TABLE II.

Due to the limited memory, the frame length is set to 40 ms, which is used for data transmission. In each frame, 16 Chirps are transmitted in 1.36 ms by each TAoC one by one, and the reflected signals are received by four RAoCs. Since the frequency of the transmitted signal is linearly increased, whereas the frequency of the received signal is fixed, the residue frequency Δf after mixer can perfectly reveal the time of flight (ToF) of electromagnetic wave, which is capable of evaluating the distance between our radar and detected subjects by extracting peak frequency components as follows:

$$d = \frac{c\Delta f T}{2B}, \tag{1}$$

where c denotes the speed of light, Δf denotes the residue frequency, $B = 2.585$ GHz denotes the bandwidth. By some algebraic manipulations, the range resolution can be given by

$$R_r = \frac{c}{2B}. \tag{2}$$

Similarly, the speed resolution can be obtained as follows:

$$V_r = \frac{c}{2BN_cT}, \tag{3}$$

where denotes the number of Chirps in a frame. Considering the frequency shift, the AD converter is set to 256 samples in each Chirp, thus the sampling rate is 3.63 M-Sample-Per-Second (MSPS).

2) Signal Processing: The collected radar data is a 4D cube containing time-domain, sampling-domain, space-domain and frame-domain information, which is illustrated in Fig. 6. For a better understanding of the collected data, we simply provide time-domain, sampling-domain, and space-domain data in a single frame as an example, which contains $16 \times 256 \times 16$ data. In signal processing, there are seven steps for three major aspects, namely large-scale activity recognition, small-scale activity recognition, and vital signs:

- **Step1:** In the beginning, the data are separated into the sample-time domain, which is a 256×16 matrix.

This article has been accepted for publication in IEEE Internet of Things Journal. This is the author's version which has not been fully edited and content may change prior to final publication. Citation information: DOI 10.1109/JIOT.2023.3336232

Then, in the first step, the fast-Fourier transform (FFT) is employed for each column, and the range-time-map can be obtained, which reveals the range between the radar and detected subjects.

- **Step2:** In **Step2**, the FFT is employed for each row in the range-time-map, and hence the range-speed-map is evaluated, which is capable of demonstrating the instantaneous speed of the detected subjects in each frame.
- **Step3:** We then compile several range-time maps in terms of the index of frames. By doing so, each row contains more activity information, i.e., if 5 frames are compiled, then the micro-doppler information in 0.2 s is included.
- **Step4:** Similarly, the FFT is employed for each row in the range-time-map generated in **Step3**, and the Range-Micro-Doppler-map can be obtained for DL algorithms to recognize the human gestures.
- **Step5:** It is not possible to create a coordinate system with only range, time and speed information. The azimuth between radar and detect subjects is also necessary. Here, the origin data cube is separated by the sample-domain and space-domain. Note that since the RAoCs are located at the same line, and by employing the Multiple Signal Classification (MUSIC) algorithm, only four space information are needed for evaluating the azimuth-map between radar and detect subjects.
- **Step6:** The low sampling signal, lower than 200 Hz, is obtained by utilizing the decimation theorem, which contains the heartbeat signal and breath-cough signal simultaneously. Then, the bandpass filters are deployed to heartbeat detection and breath-cough detection, respectively.
- **Step7:** In the end, the heartbeat per minute and the breath-cough per minute can be estimated by FFT, where the peak value reveals the number of heartbeat and breath-cough per minute.

By doing the above seven steps, the Range-Micro-Doppler-map obtained in **Step4** is able to recognize the small-scale activity, e.g., touching face or coughing. Combined range-time-map in **Step1**, range-Speed-map in **Step2** and azimuth-map in **Step5**, it is capable of recognizing the large-scale activity, i.e., one's location and its velocity. By **Step7**, the rate of heart-beat and breath-cough can be perfectly obtained. In summary, the range, speed, azimuth, micro-doppler, heartbeat, and breath-cough of detected subjects are obtained by the above seven steps, which can be employed for the proposed SSPDL.

D. HealthDAR's Algorithm

Residual network (ResNet): ResNets were first proposed by He *et al.* [39], which then achieved state-of-the-art on challenging computer vision tasks. ResNets aims to ease the training of substantially deeper networks. An important design principle of ResNets is that when the feature map size is reduced by half, the number of feature maps is doubled, maintaining the network layers' complexity. Additionally, ResNets directly use the convolution of stride = 2 for down-sampling, where it replaces the fully connected layer with the global average pool layer. A short-circuit mechanism between each two-stage layer is added to ResNet, which forms residual learning.

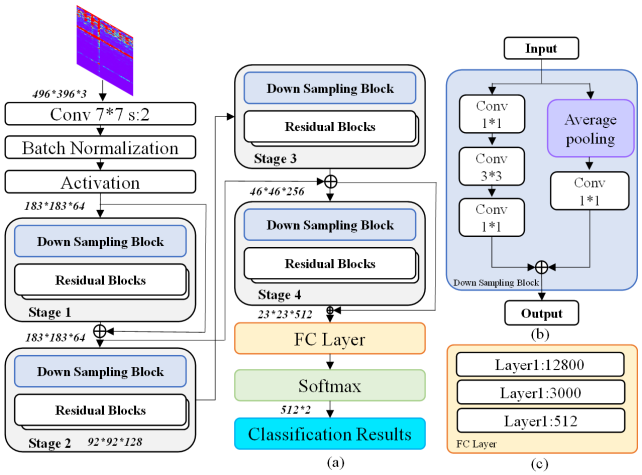

Fig. 7: The architecture of ResNet-18. (a) is the whole structure of ResNet-18, which contains four down sampling blocks, and three full connected layers. (b) is the down sampling block which contains two branches, one follows by three convolutions and the other contains one convolution. (c) is the full connected layers with three steps.

In this paper, an 18-layer ResNet is used to perform three-layer residual learning. As shown in Fig. 7, the three-layer convolution kernels are 1*1, 3*3, and 1*1, respectively. When the output and input dimensions are identical, the input and output dimensions can be directly superimposed. The full connection layer degrades the high-dimensional features into a one-dimensional vector. This work uses a three-layer full connection operation to compress the one-dimensional vector to 512 dimensions, where the final classification decision is made.

SSPDL: As shown in Fig. 8, the classification results of both signal processing and ResNet-18 are independently obtained. If two results of both signal processing and ResNet-18 are identical, the SSPDL output the final result; otherwise, both signal processing and ResNet-18 will re-classify the cough until the results are identical. More specifically, for the small-scale activities, since the SP cannot distinguish the slightly movements, the cough is classified by ResNet-18 independently. When the cough is classified successively, the vital signs can be then derived by signal processing.

III. EXPERIMENTAL EVALUATION

A. Experimental Setup

To evaluate the performance of the proposed system, we recruited three healthy student volunteers (2 women and one man) with different body conditions. During the experiments, participants wore their daily attire and face masks. To show that HealthDAR is stable no matter indoors or outdoors, we conducted our experiments in two uncontrolled environments, which are outdoors and an office room. The outdoor environment is shown in Fig. 9(a). The FMCW radar was placed

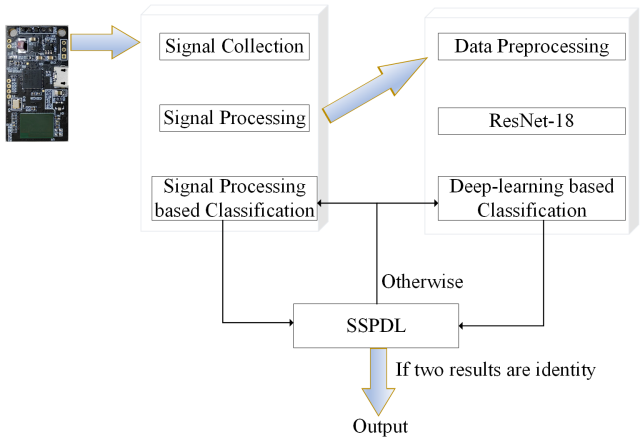

Fig. 8: SSPDL for cough detection.

within 0 to 7 m from a subject, which was located 50 cm above the ground. The office is 5.5 m $\times$ 6 m, which is a challenging scenario. As shown in Fig. 9(b), there are many desks, chairs, bookcases, and sundries. We located the radar 120 cm above the ground. It should be noted that both of two experiment environments are uncontrolled.

B. Data Collection

As shown in Table III, we categorized human activities into three main categories: 1) large-scale activity; 2) small-scale activity; 3) vital signs. The large-scale activity involves walking and running. The small-scale activity includes coughing, hand-washing, and face-touching. Vital signs hold heart rate and breath rate. We captured our data over multiple days and nights with different time spans.

Experiment for scenario 1: Our first experiment was designed to evaluate HealthDAR's ability to detect cough. During the data collection process, subjects were asked to cough while standing. Each of the subjects performed coughing and none-coughing 30 times, respectively.

Experiment for scenario 2: Our second experiment was designed to track multiple people' locations and then get the social distance of persons. Hence, firstly, we performed large-scale activities (walking and running) to test the ability of HealthDAR. Volunteers were asked to perform walking and running in casual combinations, e.g., a person was walking while another is running. The next step is to track the coughing person. We conducted the experiment where a person was coughing while another was walking/running/standing. To be

TABLE III: Classification criteria for different human activities.

	Human Activity
Large-scale activity	Walking
	Running
Small-scale activity	Coughing
	Hand-washing
	Face-touching
Vital signs	Heart rate
	Breath Rate

(a) Outdoor scenario (b) Indoor scenario

Fig. 9: Two uncontrolled experiment environments.

noted that all these experiments were conducted at different azimuths, speeds, and ranges in front of radar.

Experiment for scenario 3: Our third experiment was designed to recognize different persons' potential preventive measures. We consider 1) Indoor activities performed by one person; 2) Indoor activities performed by multiple people; 3) Outdoor activities performed by one person; 4) Outdoor activities performed by multiple people. Subjects were asked to perform hand-washing and face-touching 30 times in these four scenarios.

Experiment for new (unseen) people: We recruited 22 people to test the ability of HealthDAR on new (unseen) people, whose demographics are shown in Table IV.

Ground Truth: To determine HealthDAR's accuracy on heart rate and breath rate, we use wearable devices NeuLog sensor [40] to obtain the ground truth measurements of their breath rate and heart rate in real time. In a real-world use case, the user does not need to wear the NeuLog sensor.

C. Data Pre-processing

The data pre-processing includes time scale selection, numerical distribution analysis of micro-Doppler features, range setting and heatmap generation. More specifically, small-scale activities such as hand-washing and face-touching generally last for a short period of time. Hence, time scale is set to 0.5 s to generate micro-Doppler feature maps. Additionally, it is necessary to count the distribution characteristics of the micro-Doppler results. Based on the analysis, a certain threshold range is set to filter out these noises. A heat map dataset with a relatively uniform distribution were then generated. We finally got 6302 samples.

D. Baseline Network Parameters

We implemented two state-of-the-art baselines, which are AlexNet [41] and DenseNet-201 [42]. More specifically, for scenario 1, the DL component of SSPDL is replaced by the baselines, and the rest of HealthDAR's algorithms remained unchanged. For scenario 3, we used baselines to compare directly. AlexNet is a traditional 7-layer CNN. The convolution

TABLE IV: Demographic description of participants

Demographic data of study population	
Age (years)	20-62 years old
Gender Ratio	Male: 15, Female: 7

This article has been accepted for publication in IEEE Internet of Things Journal. This is the author's version which has not been fully edited and content may change prior to final publication. Citation information: DOI 10.1109/JIOT.2023.3336232

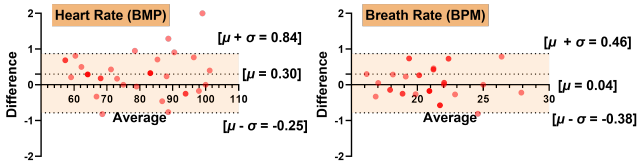

Fig. 10: Bland-Altman plot comparing HealthDAR's measurements and groundtruth when coughing.

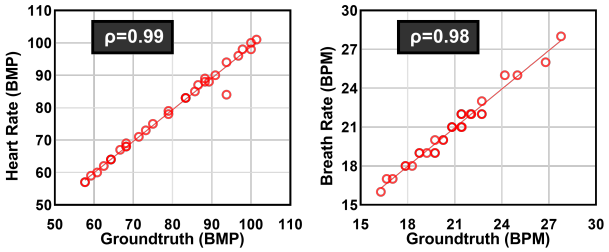

Fig. 11: Pearson correlation coefficients of HealthDAR's estimation and groundtruth when coughing.

kernel size is 3*3, and pooling layer uses 2*2 maximum pooling. The activation function is Relu, and the total number of parameters is 2.4 M. In DensNet-201, the average pooling of 2*2 is used in the transition process and the last layer of Dense. The total number of parameters reaches 8.78 M. In the forward training process, ResNet-18 uses 2*2 average pooling in the previous step of the fully connected layer, and the parameter size of ResNet-18 is 6.92 M.

E. Evaluation Metrics

The metrics used to evaluate recognition performance from different perspectives are 1) OA; 2) Recall; 3) F_1 score; and 4) Precision. The detailed description of each metric can be found in [43]. Additionally, we use the metric that is widely accepted by other studies, which consist of bias or mean error μ, standard deviation (SD) error σ and a Pearson correlation coefficient ρ.

IV. PERFORMANCE RESULTS

In this section, we evaluate the performance of HealthDAR, demonstrating its advantage over early detection, tracking, and reminding people of preventive measures. The pre-processing of radar data cube, including beam-forming and filtering, was done in MATLAB 2020b. Networks training and testing were done in Python 3.8. During the training process, we divided the pre-processing samples into three segments: 80% for the training, 10% for the validation, and 10% for testing.

A. Scenario 1: Symptom Early Detection

1) Performance of vital signs monitoring: Fig.10 shows the Bland-Altman analysis [44] that describes the average error between HealthDAR and the ground-truth. The breaths-per-minute and beats-per-minute, which refers to respiration rates

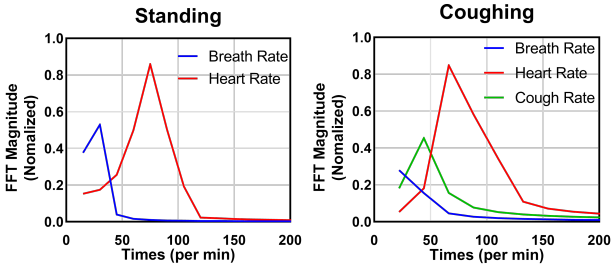

Fig. 12: An example of vital signs changing when a person is standing and coughing, respectively.

and heart rates. The mean and SD error of heart rate and breath rate when coughing are 0.3 and 0.04. In addition, the subjects' breathing rates range from 16.30 to 27.78 breaths/minute, while their heart rates vary from 57.69 to 101.4 beats/minute, where these rates span the range of adult breathing and heart rates [45]. We then computed the Pearson correlation coefficient ρ [46] to quantify the similarity between HealthDAR and the ground truth, representing the closed agreement between two variables. As shown in Fig. 11, the correlation shown of 0.99/1.0 for the heart rate and 0.98/1.0 for the breath rate represents that HealthDAR's results are highly correlated to that of the ground truth. This experimental validation demonstrated that HealthDAR could monitor subjects' vital signs properly.

2) Performance of cough detection by SSPDL model: From Fig. 12, we can easily find that when a person changed the state from standing to coughing, his vital signs changed. The first stage of our experimentation is cough detection, which distinguishes cough events from non-cough events. Table V presents the performance of cough detection using different learning methods. It can be observed from Table V that our proposed SSPDL network provides 1.000 accuracy, 1.000 recall, 1.000 precision, and 1.000 F1-score. The achieved precision by AlexNet and DenseNet-201 are 0.543 and 0.981, respectively. Results show that the accuracy of the proposed SSPDL model yields 49.7% and 1.4% improvement over AlexNet and DenseNet-201. Each baseline and SSPDL model were statistically significant at $p<0.0001$ (Wilcoxon signed-rank tests [47]). The results prove that our proposed SSPDL network is a preferable choice for cough detection.

3) Performance on new (unseen) people: In practice, high false-alarm rates stem from the confusion of coughing with similar motions, like 'bending'; or some activities have a similar pattern, like 'sneezing'. To verify this, we performed an additional experiment of cough detection on new (unseen) people. All these new (unseen) people were required 'casualty pretending coughing', e.g., performed 'bending' or 'laughing

TABLE V: Comparison of different learning models.

	OA	Precision	Recall	F1
SSPDL	1.000	1.000	1.000	1.000
AlexNet	0.503	0.543	0.500	0.519
DenseNet-201	0.986	0.981	0.991	0.986

This article has been accepted for publication in IEEE Internet of Things Journal. This is the author's version which has not been fully edited and content may change prior to final publication. Citation information: DOI 10.1109/JIOT.2023.3336232

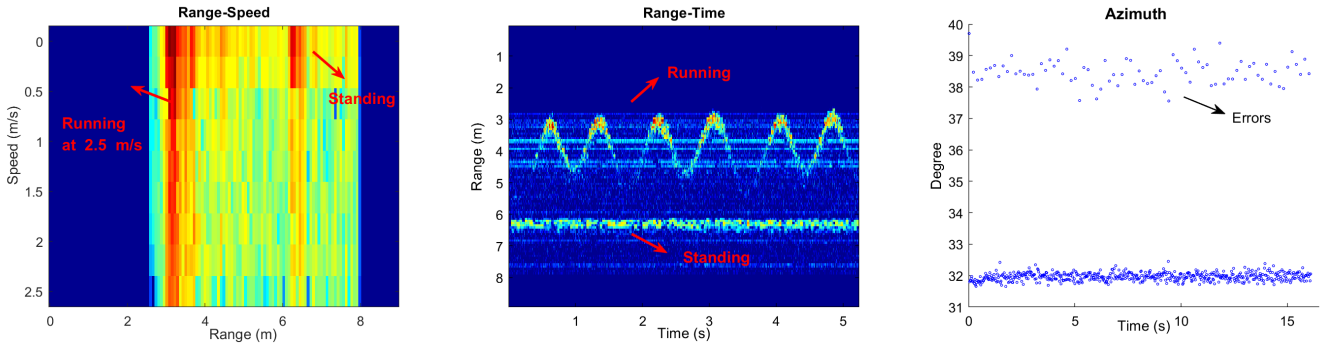

Fig. 13: Localization of multiple people. (a) Range-speed Map. (b) Range-time Map. (c) Azimuth Map.

loudly'. We compared our methods with i) Using signal processing (SP) solely; ii) Using ResNet-18 solely. An EER of 1.8% was gained with HealthDAR for cough detection. The results showed that using the proposed SSPDL network improves accuracy by 19.1 percents compared to using the SP (EER = 20.90%). For the ResNet-18 case, an EER of 15.83% was gained. There is an absolute reduction in EER of 14.03 percent, demonstrating that the proposed approach is robust on the recognition errors. Two baselines and SSPDL were statistically significant at $p<0.0001$. The OA of both networks are significantly lower than that of SSPDL, which showed the priority of our proposed method in cough detection.

4) Summary: HealthDAR could detect subjects' vital signs properly. We could achieve 100% cough recognition accuracy. Even with new (unseen) people, HealthDAR is robust against recognition errors.

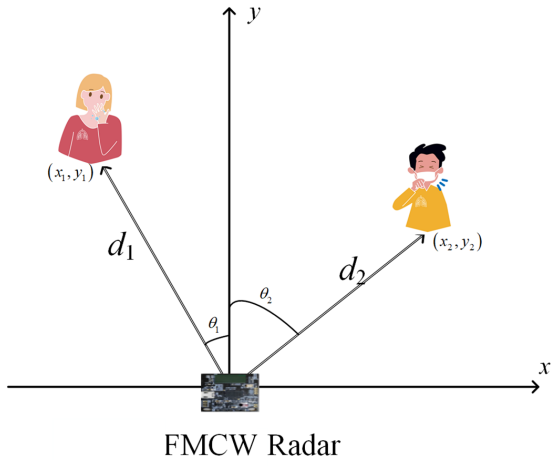

Fig. 14: An explanation for social distance.

B. Scenario 2: Tracking & Social Distancing

1) Performance of tracking: We can see from Fig. 13 (a) that *volunteer* 1 is running at a speed of 2.5 m/s from 2.5 m to 5 m forward/away from the radar while *volunteer 2* is standing and coughing at 6.25 m away from the radar. Fig. 13 (b) presents volunteer 1 running in 20 s. Additionally, from Fig. 13 (c), we correctly know his direction is 32°. Note that distinguishing standing or coughing from Fig. 13 is hard. However, by combing the SSPDL network we proposed in Section II-D, we can easily recognize his activities. Hence, with the help of HealthDAR, the average radial speeds, and the directions are correctly estimated, which leads to a perfect localization result.

2) Performance of social distancing: The social distance between two subjects can be exactly evaluated by the range and azimuth information as illustrated in Fig. 14. Firstly, the location of two detected subjects can be calculated by the Trigonometric functions, which is given by:

$$(x_1, y_1) = (d_1 \sin\theta_1, d_1 \cos\theta_1), (x_2, y_2) = (d_2 \sin\theta_2, d_2 \cos\theta_2), \tag{4}$$

where d_1 and θ_1 represent the distance and the azimuth information between radar and subject1, respectively. d_2 and θ_2 represent the distance and the azimuth information between radar and subject2, respectively. Hence, the social distance can be evaluated by the Euclidean distance between two subjects, which is written as:

$$\begin{aligned} SD &= \sqrt{(x_2 - x_1)^2 + (y_2 - y_1)^2} \\ &= \sqrt{(d_2 \sin\theta_2 - d_1 \sin\theta_1)^2 + (d_2 \cos\theta_2 - d_1 \cos\theta_1)^2}. \end{aligned} \tag{5}$$

Therefore, the social distance between two detected subjects can be readily derived.

3) Summary: In conclusion, HealthDAR could track multiple people properly, and the social distance can be correctly calculated.

C. Scenario 3: Preventive Measures

1) Performance of preventive measures recognition.: Selected range-micro-Doppler maps of hand-washing and face-touching in two uncontrolled environments are shown in Fig. 15 and Fig. 16. One can see that the noise of the outdoor environment is cleaner than that of the indoor environment, where the reflection of walls is illustrated in Fig. 16. To better illustrate the ubiquitous ability of HealthDAR, no additional SP is employed. We only used DL to extract features in these spectrograms automatically. As shown in Fig. 17, for one person, hand-washing and face-touching are correctly classified with 100% by using ResNet-18 both indoors and outdoors.

This article has been accepted for publication in IEEE Internet of Things Journal. This is the author's version which has not been fully edited and content may change prior to final publication. Citation information: DOI 10.1109/JIOT.2023.3336232

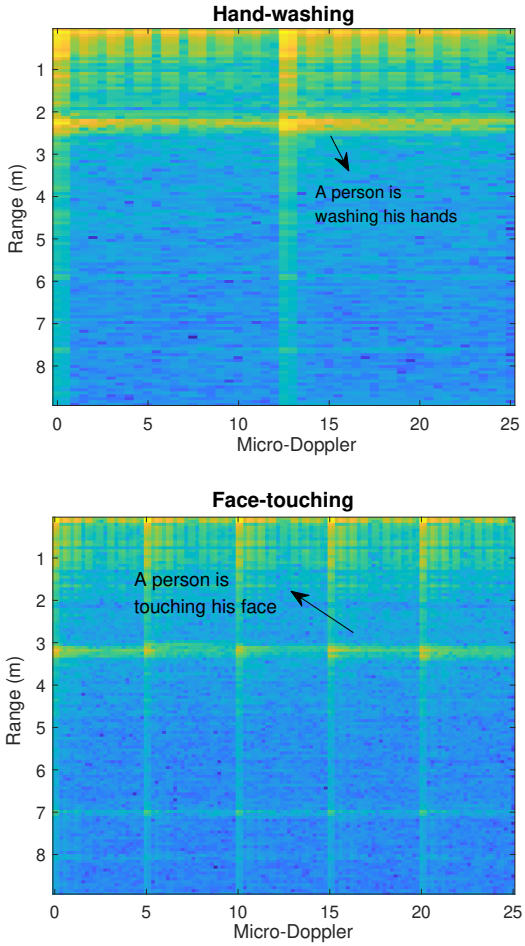

Fig. 15: Range-micro-Doppler map (outdoors).

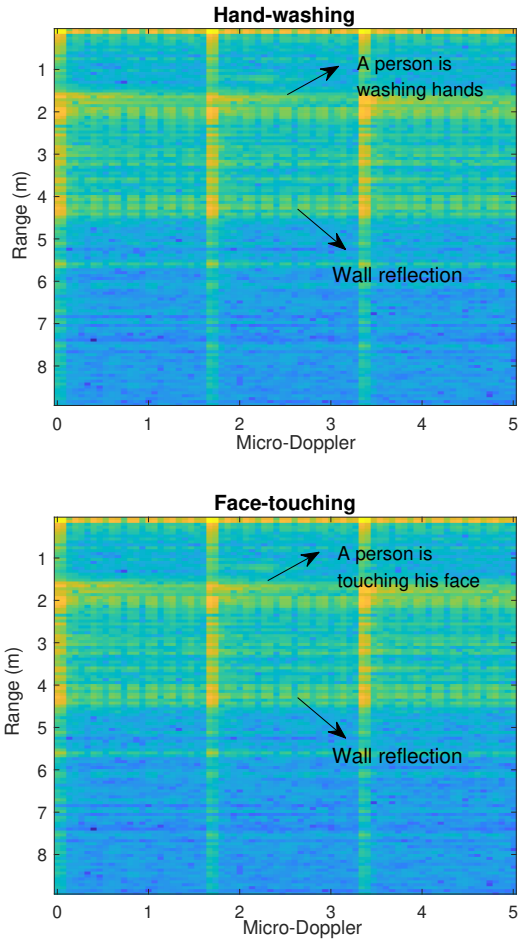

Fig. 16: Range-micro-Doppler map (indoors).

ResNet-18 achieves the best performance in the HealthDAR system (p<0.0001) compared with baseline models. Additionally, for multiple people recognition, we also achieve 100% OA, while the achieved OA by AlexNet and DenseNet-201 are 78.12%, and 86.51%, respectively. HealthDAR achieves 100% OA on both face-touching and hand-washing in both indoor and outdoor scenarios whether performed by one person or multiple people, which means that our approach is robust against the change of environment or the number of people.

2) Performance on new (unseen) people: We also tested HealthDAR's performance on new (unseen) people, which is shown in Fig. 18. We can observe that: 1) There is a drop in OA for recognizing different preventive measures on new (unseen) people. 2) The performance of outdoor scenarios outperforms that of indoor scenarios no matter by one person or multiple people. 3) The performance of face-touching is higher than that of hand-washing no matter indoors or outdoors. 4) The performance of recognizing multiple people's activities is lower than that of recognizing one person no matter indoors or outdoors. Our explanation is as follows. Firstly, outdoor performance is slightly higher than indoor performance due to its clean background, where the reflection of electromagnetic waves in the indoor scenario is much stronger than outdoor scenario. Secondly, the OA of face-touching is slightly higher than that of hand-washing because the patterns of face-touching are similar for each individual. We consider that the diversity of training samples may increase the recognition accuracy of new (unseen) people, and We would consider leaving this as an open issue in the future.

3) Summary: HealthDAR achieves 100% OA on face-touching and hand-washing in both indoor and outdoor scenarios whether performed by one person or multiple people, which means that our approach is robust against the change of environment or the number of people When tested on new (unseen) people, although HealthDAR's OA dropped by an average of 3.85%, which still achieved stable performance.

V. CONCLUSION

In this paper, we introduced HealthDAR, a coin-size system for remote health monitoring. We focused on the sensing aspect of ISAC, with a particular emphasis on remote health monitoring. We have devised a comprehensive sensing platform that employs radar technology for high-precision sensing, delivering crucial, reliable data for remote health monitoring. This platform acts as a testbed to evaluate sensing efficacy. The attractive attributes of HealthDAR are cost-effective and contactless for massive deployment, which also have no privacy

This article has been accepted for publication in IEEE Internet of Things Journal. This is the author's version which has not been fully edited and content may change prior to final publication. Citation information: DOI 10.1109/JIOT.2023.3336232

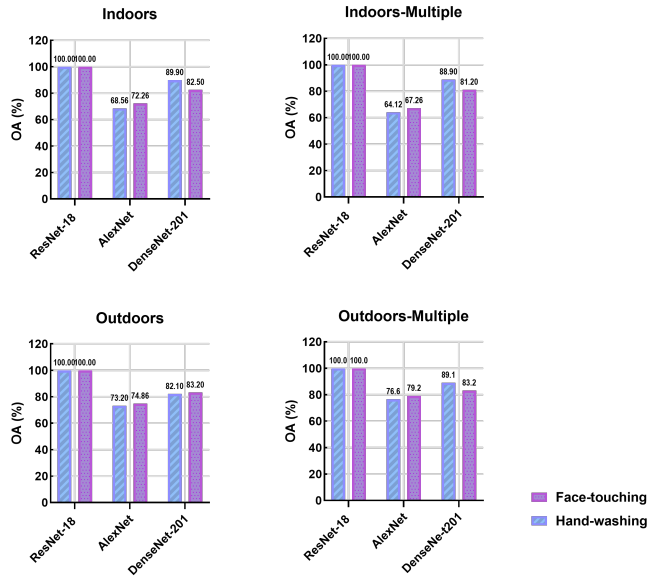

Fig. 17: Performance of one person and multiple people in indoor and outdoor scenarios, respectively.

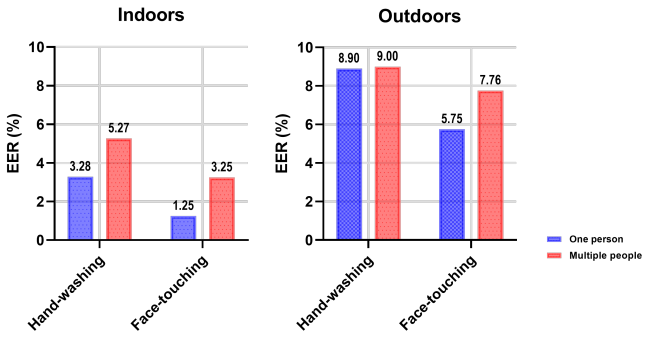

Fig. 18: Indoor and outdoor performances of hand-washing and face-touching.

issues when applied to bedrooms or bathrooms, etc. Our extensive evaluations have demonstrated the strong competence of HealthDAR in vital signs monitoring, and small-scale activity recognition in real-world scenarios.

There are several additional issues that we must consider in our future work. Due to the limited memory of our FMCW radar and the transmission rate of UART, the maximal number of Chips per frame is 16. It could be updated, and more Chirps can be saved and transmitted in a frame, which could further enhance the resolution of range, speed, micro-Doppler, heartbeat, and respiratory. Additionally, it should be noted that a potential challenge is the acceptability of society for the use of the proposed approach. A gradual adoption may be suggested starting from smaller populations such as hospitals or nursing homes to track symptom evolution or as part of telemedicine and individual uses, then scaling it to higher volumes. Our proposed system would enable remote diagnosis and treatment monitoring of patients, thereby helping to reduce direct contact with medical staff. Our proposed system would also improve the health monitoring of people at home. Tracking data collected through such a system could also provide valuable information. This work also has potential value in applications involving personal identity verification, human-machine interfaces, disability assistance, rehabilitation, and biomedical engineering.

REFERENCES

[1] X. Li, Y. Cui, J. A. Zhang, F. Liu, D. Zhang, and L. Hanzo, "Integrated human activity sensing and communications," *IEEE Communications Magazine*, vol. 61, no. 5, pp. 90–96, 2023.

[2] S. Khan, F. Luo, Z. Zhang, F. Ullah, F. Amin, S. F. Qadri, M. B. B. Heyat, R. Ruby, L. Wang, S. Ullah *et al.*, "A survey on x. 509 public-key infrastructure, certificate revocation, and their modern implementation on blockchain and ledger technologies," *IEEE Communications Surveys & Tutorials*, 2023.

[3] J. Pegoraro *et al.*, "Human sensing with mmwave systems: from radar to integrated sensing and communication," 2023.

[4] H. C. Ates, A. K. Yetisen, F. Güder, and C. Dincer, "Wearable devices for the detection of covid-19," *Nature Electronics*, vol. 4, no. 1, pp. 13–14, 2021.

[5] X. Zeng and Q. Sun, "Guest editorial: Intelligent wearable systems for human health monitoring," *IEEE Transactions on Industrial Informatics*, vol. 16, no. 11, pp. 7136–7137, 2020.

[6] G. Yang, L. Xie, M. Mäntysalo, X. Zhou, Z. Pang, L. D. Xu, S. Kao-Walter, Q. Chen, and L.-R. Zheng, "A health-iot platform based on the integration of intelligent packaging, unobtrusive bio-sensor, and intelligent medicine box," *IEEE Transactions on Industrial Informatics*, vol. 10, no. 4, pp. 2180–2191, 2014.

[7] P. Sapiezynski, A. Stopczynski, D. K. Wind, J. Leskovec, and S. Lehmann, "Inferring person-to-person proximity using wifi signals," *Proceedings of the ACM on Interactive, Mobile, Wearable and Ubiquitous Technologies*, vol. 1, no. 2, pp. 1–20, 2017.

[8] S. Gerke, C. Shachar, P. R. Chai, and I. G. Cohen, "Regulatory, safety, and privacy concerns of home monitoring technologies during covid-19," *Nature medicine*, vol. 26, no. 8, pp. 1176–1182, 2020.

[9] A. Li, E. Bodanese, S. Poslad, T. Hou, F. Luo, and K. Wu, "Trajectory-based fall detection and recognition using ultra-wideband signals," in *GLOBECOM 2022 - 2022 IEEE Global Communications Conference*, 2022, pp. 2260–2265.

[10] A. Li, E. Bodanese, S. Poslad, Z. Huang, T. Hou, K. Wu, and F. Luo, "An integrated sensing and communication system for fall detection and recognition using ultra-wideband signals," *IEEE Internet of Things Journal*, pp. 1–1, 2023.

[11] W. Li, Y. Chai, F. Khan, S. R. U. Jan, S. Verma, V. G. Menon, f. Kavita, and X. Li, "A comprehensive survey on machine learning-based big data analytics for iot-enabled smart healthcare system," *Mobile networks and applications*, vol. 26, pp. 234–252, 2021.

[12] M. Mercuri, I. R. Lorato, Y.-H. Liu, F. Wieringa, C. V. Hoof, and T. Torfs, "Vital-sign monitoring and spatial tracking of multiple people using a contactless radar-based sensor," *Nature Electronics*, vol. 2, no. 6, pp. 252–262, 2019.

[13] C. Liu, J. Xiong, L. Cai, L. Feng, X. Chen, and D. Fang, "Beyond respiration: Contactless sleep sound-activity recognition using rf signals," *Proceedings of the ACM on Interactive, Mobile, Wearable and Ubiquitous Technologies*, vol. 3, no. 3, pp. 1–22, 2019.

[14] P. Sharma, X. Hui, and E. C. Kan, "A wearable rf sensor for monitoring respiratory patterns," in *2019 41st Annual International Conference of the IEEE Engineering in Medicine and Biology Society (EMBC)*. IEEE, 2019, pp. 1217–1223.

[15] S. Khan, F. Luo, Z. Zhang, M. A. Rahim, M. Ahmad, and K. Wu, "Survey on issues and recent advances in vehicular public-key infrastructure (vpki)," *IEEE Communications Surveys & Tutorials*, vol. 24, no. 3, pp. 1574–1601, 2022.

[16] S. Z. Gurbuz and M. G. Amin, "Radar-based human-motion recognition with deep learning: Promising applications for indoor monitoring," *IEEE Signal Processing Magazine*, vol. 36, no. 4, pp. 16–28, 2019.

[17] C. Li, V. M. Lubecke, O. Boric-Lubecke, and J. Lin, "A review on recent advances in doppler radar sensors for noncontact healthcare monitoring,"

IEEE Transactions on microwave theory and techniques, vol. 61, no. 5, pp. 2046–2060, 2013.
[18] J. Wang, N. Varshney, C. Gentile, S. Blandino, J. Chuang, and N. Golmie, "Integrated sensing and communication: Enabling techniques, applications, tools and data sets, standardization, and future directions," *IEEE Internet of Things Journal*, vol. 9, no. 23, pp. 23 416–23 440, 2022.
[19] M. Rihan, A. Zappone, S. Buzzi, G. Fodor, and M. Debbah, "Passive vs. active reconfigurable intelligent surfaces for integrated sensing and communication: Challenges and opportunities," *IEEE Network*, pp. 1–1, 2023.
[20] S. Lai, N. W. Ruktanonchai, L. Zhou, O. Prosper, W. Luo, J. R. Floyd, A. Wesolowski, M. Santillana, C. Zhang, X. Du *et al.*, "Effect of non-pharmaceutical interventions to contain covid-19 in china," *nature*, vol. 585, no. 7825, pp. 410–413, 2020.
[21] A. Hafeez, S. Ahmad, S. A. Siddqui, M. Ahmad, and S. Mishra, "A review of covid-19 (coronavirus disease-2019) diagnosis, treatments and prevention," *EJMO*, vol. 4, no. 2, pp. 116–125, 2020.
[22] A. Repici, R. Maselli, M. Colombo, R. Gabbiadini, M. Spadaccini, A. Anderloni, S. Carrara, A. Fugazza, M. Di Leo, P. A. Galtieri *et al.*, "Coronavirus (covid-19) outbreak: what the department of endoscopy should know," *Gastrointestinal endoscopy*, vol. 92, no. 1, pp. 192–197, 2020.
[23] I. D. Miranda, A. H. Diacon, and T. R. Niesler, "A comparative study of features for acoustic cough detection using deep architectures," in *2019 41st Annual International Conference of the IEEE Engineering in Medicine and Biology Society (EMBC)*. IEEE, 2019, pp. 2601–2605.
[24] E. A. Mohammed, M. Keyhani, A. Sanati-Nezhad, S. H. Hejazi, and B. H. Far, "An ensemble learning approach to digital corona virus preliminary screening from cough sounds," *Scientific Reports*, vol. 11, no. 1, pp. 1–11, 2021.
[25] S. Adavanne, A. Politis, and T. Virtanen, "Direction of arrival estimation for multiple sound sources using convolutional recurrent neural network," in *2018 26th European Signal Processing Conference (EUSIPCO)*. IEEE, 2018, pp. 1462–1466.
[26] G.-T. Lee, H. Nam, S.-H. Kim, S.-M. Choi, Y. Kim, and Y.-H. Park, "Deep learning based cough detection camera using enhanced features," *arXiv preprint arXiv:2107.13260*, 2021.
[27] R. X. A. Pramono, S. A. Imtiaz, and E. Rodriguez-Villegas, "A cough-based algorithm for automatic diagnosis of pertussis," *PloS one*, vol. 11, no. 9, p. e0162128, 2016.
[28] J. Laguarta, F. Hueto, and B. Subirana, "Covid-19 artificial intelligence diagnosis using only cough recordings," *IEEE Open Journal of Engineering in Medicine and Biology*, vol. 1, pp. 275–281, 2020.
[29] A. Gollwitzer, C. Martel, W. J. Brady, P. Pärnamets, I. G. Freedman, E. D. Knowles, and J. J. Van Bavel, "Partisan differences in physical distancing are linked to health outcomes during the covid-19 pandemic," *Nature human behaviour*, vol. 4, no. 11, pp. 1186–1197, 2020.
[30] J. J. Van Bavel, A. Cichocka, V. Capraro, H. Sjåstad, J. B. Nezlek, T. Pavlović, M. Alfano, M. J. Gelfand, F. Azevedo, M. D. Birtel *et al.*, "National identity predicts public health support during a global pandemic," *Nature communications*, vol. 13, no. 1, pp. 1–14, 2022.
[31] K. Leung, J. T. Wu, and G. M. Leung, "Real-time tracking and prediction of covid-19 infection using digital proxies of population mobility and mixing," *Nature communications*, vol. 12, no. 1, pp. 1–8, 2021.
[32] X. Song, B. Yang, G. Yang, R. Chen, E. Forno, W. Chen, and W. Gao, "Spirosonic: monitoring human lung function via acoustic sensing on commodity smartphones," in *Proceedings of the 26th Annual International Conference on Mobile Computing and Networking*, 2020, pp. 1–14.
[33] M. Pahar, M. Klopper, R. Warren, and T. Niesler, "Covid-19 cough classification using machine learning and global smartphone recordings," *Computers in Biology and Medicine*, vol. 135, p. 104572, 2021.
[34] J. Chen, K. Li, Z. Zhang, K. Li, and P. S. Yu, "A survey on applications of artificial intelligence in fighting against covid-19," *ACM Computing Surveys (CSUR)*, vol. 54, no. 8, pp. 1–32, 2021.
[35] F. Lin, Y. Zhuang, C. Song, A. Wang, Y. Li, C. Gu, C. Li, and W. Xu, "Sleepsense: A noncontact and cost-effective sleep monitoring system," *IEEE Transactions on Biomedical Circuits and Systems*, vol. 11, no. 1, pp. 189–202, 2017.
[36] A. D. Singh, S. S. Sandha, L. Garcia, and M. Srivastava, "Radhar: Human activity recognition from point clouds generated through a millimeter-wave radar," in *Proceedings of the 3rd ACM Workshop on Millimeter-wave Networks and Sensing Systems*, 2019, pp. 51–56.
[37] X. Li, Y. He, F. Fioranelli, and X. Jing, "Semisupervised human activity recognition with radar micro-doppler signatures," *IEEE Transactions on Geoscience and Remote Sensing*, 2021.
[38] IWR1642Boost, Texas Instruments company. [Online]. Available: https://www.ti.com/sensors/mmwave-radar/overview.html.
[39] K. He, X. Zhang, S. Ren, and J. Sun, "Deep residual learning for image recognition," in *Proceedings of the IEEE Conference on Computer Vision and Pattern Recognition (CVPR)*, June 2016.
[40] [Online]. Available: https://neulog.com/
[41] A. Krizhevsky, I. Sutskever, and G. E. Hinton, "Imagenet classification with deep convolutional neural networks," *Advances in neural information processing systems*, vol. 25, 2012.
[42] S.-H. Wang and Y.-D. Zhang, "Densenet-201-based deep neural network with composite learning factor and precomputation for multiple sclerosis classification," *ACM Transactions on Multimedia Computing, Communications, and Applications (TOMM)*, vol. 16, no. 2s, pp. 1–19, 2020.
[43] G. Forman *et al.*, "An extensive empirical study of feature selection metrics for text classification." *J. Mach. Learn. Res.*, vol. 3, no. Mar, pp. 1289–1305, 2003.
[44] D. Giavarina, "Understanding bland altman analysis," *Biochemia medica*, vol. 25, no. 2, pp. 141–151, 2015.
[45] F. Adib, H. Mao, Z. Kabelac, D. Katabi, and R. C. Miller, "Smart homes that monitor breathing and heart rate," in *Proceedings of the 33rd annual ACM conference on human factors in computing systems*, 2015, pp. 837–846.
[46] J. Benesty, J. Chen, Y. Huang, and I. Cohen, "Pearson correlation coefficient," in *Noise reduction in speech processing*. Springer, 2009, pp. 1–4.
[47] R. F. Woolson, "Wilcoxon signed-rank test," *Wiley encyclopedia of clinical trials*, pp. 1–3, 2007.

Anna Li received her PhD degree in Computer Science from Queen Mary University of London in 2023. She is currently a lecturer in the School of Computing and Communications at Lancaster University. Her research interests include human activity recognition, signal processing, wireless communication, sensor systems, deep learning, and integrated navigation and communications. Dr. Li is passionate about creating innovative and accessible technologies that promote human health and well-being.

Eliane Bodanese MSc, Ph.D., MIEEE, joined Queen Mary University of London in 2003. She is a senior lecturer at the School of Electronic Engineering and Computer Science and a member of the Networks Research Group. She received her Electrical Engineering degree from the Federal University of Parana (Brazil) and her M.Sc. degree in Electrical Engineering from the Federal University of Santa Catarina (Brazil). She received her Ph.D. in Electronic Engineering from Queen Mary, University of London (UK). Her research interests include the Internet of Things, human activity detection and recognition through nonintrusive sensing, indoor/outdoor localization, communication support for emergencies, heterogeneous and cooperative communications. She is a reviewer of numerous journals including IEEE Transactions on Communications, IEEE Sensors Journal, IEEE IoT Journal, and IEEE Transactions on Intelligent Transportation Systems.

This article has been accepted for publication in IEEE Internet of Things Journal. This is the author's version which has not been fully edited and content may change prior to final publication. Citation information: DOI 10.1109/JIOT.2023.3336232

Stefan Poslad has a Ph.D. in medical sensing. He is in the School of Electronic Engineering and Computer Science, Queen Mary University of London, where he is director of the QMUL IoT Lab. His research and teaching interests include ubiquitous computing, Internet of Things (IoT); smart environments, artificial intelligence and distributed systems. He has been the lead researcher for QMUL on over 15 international collaborative projects with industry, across the transport, health and environment science domains.

Penghui Chen received the B.S. and Ph.D. degree from Beihang University, Beijing, China, in 2007 and 2013, respectively. He carried out his Post Doctor research from 2013 to 2015 in Beihang University, where he is currently a Lecturer. His research interests include fast calculation techniques of electromagnetic scattering characteristics, radar target recognition, millimeter wave radar signal processing and applications.

Jun Wang received the B.S. degree from the Northwestern Polytechnical University, Xian, China, in 1995 and the M.S. and Ph.D. degrees from Beihang University (BUAA), Beijing, China, in 1998 and 2001, respectively. He is currently a professor with the School of Electronic and Information Engineering, BUAA. His main research interests are signal processing, DSP/FPGA real time architecture, target recognition and tracking.

Yonglei Fan received BSc and MSc from South China Normal University and University of Chinese Academy of Sciences, China. He is currently pursuing a Ph.D. degree in Computer Science at Queen Mary University of London, London, UK. His research interests are Geographical Information Science, indoor poisoning technique, human activity recognition and Internet of Things.

Tianwei Hou (S'19—M'21) received Ph.D. degree from Beijing Jiaotong University (BJTU) in 2021. He was a visiting scholar at Queen Mary University of London (QMUL) (Sep. 2018- Nov. 2020). Since 2021, he has been an associate professor at BJTU. Dr. Hou's current research interests include next generation multiple access (NGMA), reconfigurable intelligent surface (RIS) aided communications, UAV communications, multiuser multiple-input multiple-output (MIMO) communications, and stochastic geometry. He has granted a Marie Sklodowska-Curie fellowship by European Research Executive Agency in 2023. He has been selected as a young elite scientist sponsorship program by China Association for Science and Technology in 2022. He received the Exemplary Reviewer of the IEEE COMMUNICATION LETTERS and the IEEE TRANSACTIONS ON COMMUNICATIONS in 2018, 2019 and 2022. He has served as a TPC Member for many IEEE conferences, such as GLOBECOM, VTC, etc. He served as the publicity officer for the Next Generation Multiple Access Emerging Technology Initiative (NGMA-ETI). He has served as a Co-Chair in the 2nd, 4th and 5th NGMA-for-future-wireless-communication workshops in IEEE VTC 2022-Fall, IEEE VTC 2023-spring, IEEE ISCT-2022 and IEEE PIMRC 2023. He has also served as a co-chair in the RIS and Smart Environments Symposium of IEEE ICCT 2023. He serves as the leading Guest Editor for IEEE IoT-J special issue on Next Generation Multiple Access for Internet of Things.